



LAWRENCE  
LIVERMORE  
NATIONAL  
LABORATORY

# The hydration, microstructure, and mechanical properties of vaterite calcined clay cement (VC3)

J. Li, Y. Li

May 11, 2023

Cement and Concrete Research

## **Disclaimer**

---

This document was prepared as an account of work sponsored by an agency of the United States government. Neither the United States government nor Lawrence Livermore National Security, LLC, nor any of their employees makes any warranty, expressed or implied, or assumes any legal liability or responsibility for the accuracy, completeness, or usefulness of any information, apparatus, product, or process disclosed, or represents that its use would not infringe privately owned rights. Reference herein to any specific commercial product, process, or service by trade name, trademark, manufacturer, or otherwise does not necessarily constitute or imply its endorsement, recommendation, or favoring by the United States government or Lawrence Livermore National Security, LLC. The views and opinions of authors expressed herein do not necessarily state or reflect those of the United States government or Lawrence Livermore National Security, LLC, and shall not be used for advertising or product endorsement purposes.

---

1 The hydration, microstructure, and mechanical properties of vaterite calcined clay cement (VC<sup>3</sup>)

2  
3 Yaqiang Li <sup>1,\*</sup>, Yue Li <sup>2,\*</sup>, Hongyan Ma <sup>3</sup>, Jiaqi Li <sup>4,\*</sup>

4  
5 <sup>1</sup> Department of Civil Engineering, Beijing Forestry University, Beijing 100083, China.

6 <sup>2</sup> The Key Laboratory of Urban Security and Disaster Engineering, MOE. Beijing University of  
7 Technology, Beijing 100124, PR China.

8 <sup>3</sup> Missouri University of Science & Technology, Department of Civil Architectural &  
9 Environmental Engineering, Rolla, MO 65409 United States.

10 <sup>4</sup> Atmospheric, Earth, and Energy Division, Lawrence Livermore National Laboratory,  
11 Livermore 94550, United States.

12  
13 \* Corresponding author: Yaqiang Li; Yue Li; Jiaqi Li

14 E-mail address: [liyaqiang@bjfu.edu.cn](mailto:liyaqiang@bjfu.edu.cn) (Y. Li); [liyue@bjut.edu.cn](mailto:liyue@bjut.edu.cn) (Y. Li); [li88@llnl.gov](mailto:li88@llnl.gov) (J. Li).

15  
16 Abstract: Limestone (calcite) calcined clay cement (LC<sup>3</sup>) is a promising low-CO<sub>2</sub> binder, but the  
17 low activity of calcite cannot compensate the reduction in clinker factor, resulting in low one-day  
18 strength and limiting its broad applications. As recent carbon capture and utilization technologies  
19 allow scalable production of vaterite, a more reactive CaCO<sub>3</sub> polymorph, we overcome the  
20 challenge by introducing vaterite calcined clay cement (VC<sup>3</sup>), inspired by the vaterite-calcite  
21 phase change. In the present study, VC<sup>3</sup> exhibits higher compressive strengths and faster  
22 hydration than LC<sup>3</sup>. Compared to hydrated LC<sup>3</sup>, hydrated VC<sup>3</sup> exhibits increased amount of  
23 hemi- and mono-carboaluminate formation and decreased amount of strätlingite formation. With  
24 gypsum adjustment, the 1-day strength of VC<sup>3</sup> is higher than that of pure cement reference. VC<sup>3</sup>,  
25 a low-CO<sub>2</sub> binder, presents great potential as a host of the metastable CaCO<sub>3</sub> for carbon storage  
26 and utilization and as an enabler of carbon capture at gigaton scales.

27  
28 Keywords: carbon utilization; carbon storage; CCUS; bio-inspired; low-CO<sub>2</sub> cement.

## 29 30 1. Introduction

31 Portland cement is the most versatile binder in construction, with current production of over  
32 4 Gt/year and a projected increase in demand by 50% [1]. The massive cement production  
33 accounts for ~8% of global anthropogenic CO<sub>2</sub> emissions [2]. As the second largest commodity  
34 after freshwater, the decarbonization of cement is of great interest but great challenges as well.  
35 Gigaton-scale decarbonization by alternative or blended low-carbon cement is handicapped by  
36 economic viability, technical feasibility, and scalability (e.g., raw materials distribution) [3].

37 Most modern cement kilns are at or close to the maximum thermal efficiency [4]; thus,  
38 decarbonization strategies have focused on exploring materials alternative or supplementary to  
39 cement. The partial cement clinker replacement by supplementary cementitious materials (SCMs,  
40 e.g., coal fly ash) is a mature cement decarbonization strategy [5]. However, due to the global  
41 energy transition, in recent years, byproduct SCMs from other industries (e.g., fly ash from coal  
42 power plants and granulated blast furnace slag from iron manufacturing) could not meet the  
43 massive cement demand [6]. With the high natural reservoir capacity of limestone (calcite),  
44 limestone calcined clay cement (LC<sup>3</sup>) has been widely validated as a scalable, low-cost solution  
45 to cement decarbonization at a clinker content of up to 50% [7, 8]. Both limestone and clay are  
46 locally available and massively sourced at low costs. LC<sup>3</sup> with 50% clinker replacement can

---

47 achieve equivalent strengths to ordinary Portland cement by 3 days [9], exhibiting higher late-age  
48 mechanical properties due to refined microstructure by reactions between clinker / hydrates,  
49 limestone, and calcined clay (mainly metakaolin) [10]. Besides calcium aluminosilicate hydrate  
50 (C-A-S-H), other major reaction products (i.e., hemicarboaluminate, monocarboaluminate, and  
51 strätlingite) also play important roles in the enhanced durability of LC<sup>3</sup> [11]. Requiring no special  
52 handling or training, LC<sup>3</sup> technology has been readily deployable at scale [12].

53 Despite many advantages and industrial interests [13], LC<sup>3</sup> presents unignorable limitations:  
54 1) low early-age strengths (e.g., at 1 day) [14]; 2) complex rheology (e.g., poor flowability) [15];  
55 and 3) production slowdown due to enhanced needs for grinding specific components of LC<sup>3</sup>.  
56 While inter-grinding clinker, gypsum, calcined clay, and limestone using mills does not reduce  
57 the productivity of blended cement, the particle size distribution of each component of LC<sup>3</sup> is  
58 difficult to optimize and affects productivity. Thus, the common strategy, e.g., in the U.S.  
59 markets, is instead inter-blending where Portland cement, calcined clay, and limestone are  
60 individually ground to the required fineness and blended together [16], compromising the  
61 production rate.

62 The low 1-day strength of LC<sup>3</sup> may be mitigated by chloride-based [17] or calcium silicate  
63 hydrate (C-S-H) seed-based accelerators [18]. However, using such accelerators limits the use of  
64 LC<sup>3</sup> concrete to non-reinforced applications or at low water-to-cement ratios [17, 19]. The  
65 abovementioned limitations may be resolved simultaneously with the new ternary Portland  
66 cement system – vaterite calcined clay cement (VC<sup>3</sup>), in which the limestone powders of LC<sup>3</sup> are  
67 replaced by vaterite, a metastable CaCO<sub>3</sub> polymorph with a higher reactivity in Ca-rich  
68 cementitious systems, compared to calcite [20]. Additionally, the spherical nature of vaterite  
69 particles mitigates the flowability issue associated with LC<sup>3</sup>. Recent advances in the deployment  
70 of climate technology (e.g., by Calera and Fortera) allow low-cost production of vaterite at scale  
71 with co-benefits of air CO<sub>2</sub> capture or point source carbon capture [21]. The global warming  
72 potential of vaterite production through carbon storage depends on the carbon footprint of energy  
73 use (e.g., renewable electricity), CO<sub>2</sub> capture efficiency, raw materials, and type of processes.  
74 Via the “climate tech” pioneers, the embodied carbon of vaterite production could be down to  
75 0.3 kg CO<sub>2</sub> per kg of vaterite produced, while stoichiometrically, 1 kg of vaterite can store 0.44  
76 kg of CO<sub>2</sub>. Thus, vaterite can be potentially produced at an overall “negative” carbon  
77 embodiment (i.e., -0.14 kg CO<sub>2</sub>/kg vaterite).

78 A proof-of-concept study is needed for the potential outperformance of VC<sup>3</sup> over LC<sup>3</sup>.  
79 Although VC<sup>3</sup> is similar to LC<sup>3</sup> at first glance, metastable vaterite may alter the chemistry and  
80 microstructure of the ternary blended cement system and late-age strengths (e.g., at 28 days). The  
81 following intriguing questions remain unknown: 1) does the more reactive CaCO<sub>3</sub> polymorph  
82 increase the formation of hemi- or mono- carboaluminate? 2) does the competition for aluminum  
83 in metakaolin limit the formation of strätlingite? and 3) does vaterite lead to higher 28-day  
84 strengths of VC<sup>3</sup> relative to LC<sup>3</sup>?

85 In this study, we investigated the properties of vaterite and metakaolin-blended Portland  
86 cement as the prove-of-concept for the proposed VC<sup>3</sup> at a clinker content of ~50%. While  
87 applying comparable particle sizes of CaCO<sub>3</sub>, we examined the mechanical properties, hydration,  
88 and microstructure of our VC<sup>3</sup> system and compared with those of the classic LC<sup>3</sup> system. To  
89 verify improved early-age performance, the hydrated VC<sup>3</sup> and LC<sup>3</sup> (same metakaolin-to-CaCO<sub>3</sub>  
90 mass ratio of 2) at 1-day age were characterized using X-ray diffraction (XRD), scanning  
91 electron microscopy (SEM), calorimetry, and thermogravimetric analysis (TGA). The

92 compressive strengths of VC<sup>3</sup> were optimized by sulfation adjustment and measured up to 28  
 93 days.

94 The present work unveils the chemistry and materials properties of the new low-CO<sub>2</sub>  
 95 ternary blended system, VC<sup>3</sup>, and motivates continued studies on VC<sup>3</sup> durability and rheology,  
 96 inspires the development of vaterite-rich blended cement, and provides implications for gigaton-  
 97 scale enablers of air CO<sub>2</sub> capture and storage as well as point source carbon capture and storage.

98  
 99 2. Materials and methods

100 2.1 Materials

101 Type I ordinary Portland cement (OPC) was used in this study. Metakaolin with >96%  
 102 purity was obtained from BASF Metamax. Vaterite was synthesized following the protocol in  
 103 [22, 23]. Briefly, vaterite was prepared by mixing CaCl<sub>2</sub> and Na<sub>2</sub>CO<sub>3</sub> aqueous solutions at a  
 104 molar ratio of 1:1 at 25 °C, followed by 1 min of centrifuging at 5000 rpm. The precipitate was  
 105 rinsed with ethanol and dried at 50 °C for 12 h. Calcite was prepared by ball-milling limestone  
 106 powder for 30 minutes. Details of the chemical compositions and physical properties of raw  
 107 materials are given in **Table 1**, **Table 2**, and **Fig. 1**. Calcite (>99% purity) shows slightly smaller  
 108 D50 compared to vaterite (>95% purity) but a broader range of particle size distribution. **Fig. 2**  
 109 shows the morphology of calcite and vaterite. The vaterite synthesized in this study is  
 110 morphologically similar to that prepared from carbon capture [21]. A polycarboxylate ether  
 111 (PCE)-based superplasticizer (powder, SIKA) was used to ensure optimal workability for  
 112 selected mix proportions.

113  
 114 **Table 1** Chemical compositions of ordinary Portland cement and metakaolin used in this study.

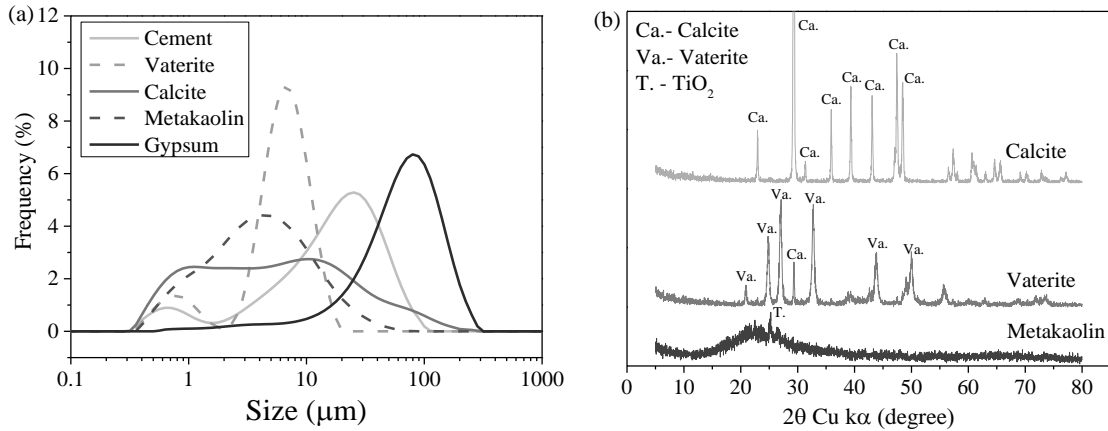
Oxides	OPC (%)	Metakaolin (%)	Crystalline phases of OPC	Content (%)
CaO	67.36	0.02	C <sub>3</sub> S	61.28
SiO <sub>2</sub>	19.04	51.96	C <sub>2</sub> S	18.43
Fe <sub>2</sub> O <sub>3</sub>	3.74	0.46	C <sub>3</sub> A	5.85
SO <sub>3</sub>	3.22	0.06	C <sub>4</sub> AF	7.94
Al <sub>2</sub> O <sub>3</sub>	3.16	44.34	Gypsum (C\$H <sub>2</sub> )	3.65
MgO	1.67	0.00	Dolomite	1.28
K <sub>2</sub> O	0.66	0.11	Periclase	0.64
TiO <sub>2</sub>	0.60	2.65	Quartz	0.42
Na <sub>2</sub> O	0.29	0.25	Calcite	0.51
MnO	0.07	0.00	/	/
LOI	0.19	0.15	/	/

115 Note: LOI = Loss on ignition; Cement notation: C = CaO, S = SiO<sub>2</sub>, A = Al<sub>2</sub>O<sub>3</sub>, F = Fe<sub>2</sub>O<sub>3</sub>, \$ = SO<sub>3</sub>, H = H<sub>2</sub>O.

116  
 117 **Table 2** Particle size distribution, specific surface area, and specific gravity of raw materials.

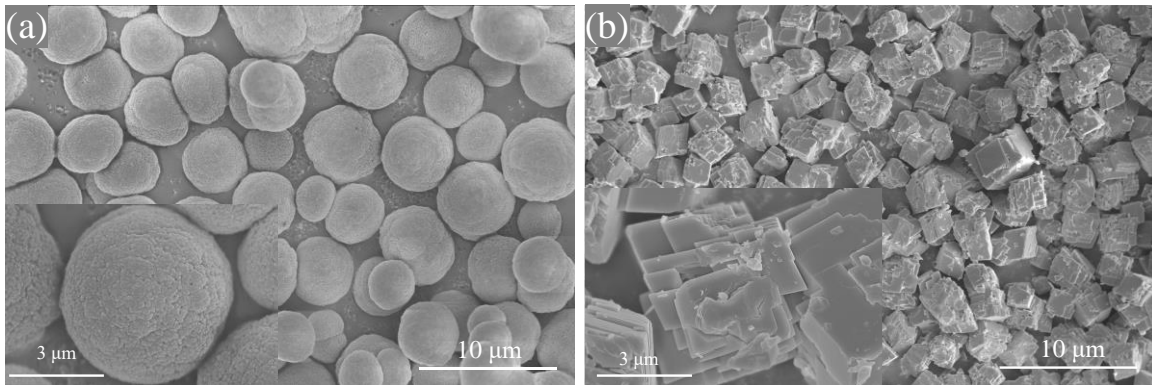
Materials	D10 (µm)	D50 (µm)	D90 (µm)	Specific surface area (m <sup>2</sup> /g)	Density (g/cm <sup>3</sup> )
Cement	2.41	16.95	44.42	1.27	3.1
Vaterite	1.08	5.92	10.52	65.72	2.54
Calcite	0.75	5.04	35.95	2.78	2.71
Metakaolin	0.93	3.75	13.13	21.62	2.23
Gypsum	18.65	64.60	140.22	0.24	2.32

118



119  
120  
121  
122

**Fig.1** Particle size distribution and diffraction patterns of raw materials. (a) Particle size distribution; (b) XRD patterns.



123  
124  
125  
126  
127  
128  
129  
130

**Fig.2** SEM micrographs of vaterite and calcite showing distinct morphologies. (a) Vaterite; (b) Calcite.

The mix proportions and the nomenclature used in this study are given in **Table 3**. Coupled substitutions of metakaolin and calcite or vaterite were mixed at the mass ratio 2:1.

**Table 3** Mix proportions used in this study.

	OPC (g)	Calcite (g)	Vaterite (g)	Metakaolin (g)	Gypsum (g)	Water (g)	PCE (g)
OPC	100	-	-	-	-	50	-
PLC	85	15	-	-	-	50	-
PVC	85	-	15	-	-	50	-
LC <sup>3</sup>	55	15	-	30	-	50	0.2
VC <sup>3</sup>	55	-	15	30	-	50	0.2
VC <sup>3</sup> -1.5C\$	54.175	-	14.775	29.55	1.3	50	0.2
VC <sup>3</sup> -3.0C\$	53.35	-	14.55	29.1	3	50	0.2

131  
132  
133  
134  
135

## 2.2 Methods

For preparing blended cement pastes, the powders were first dry-mixed at 25 °C for 1 min at 150 rpm, followed by the mixing with water and superplasticizer for 3 min at 300 rpm. All pastes were cast at a water-to-binder (w/b) ratio of 0.5 at 25 °C.

136 The flowability (mini-slump) test follows the protocol in [24]. The test was conducted by  
137 placing a moistened cone on a moistened flat plate. The dimensions of the top and bottom rims  
138 and the height of the moistened cone are 36 mm, 60 mm, and 60 mm, respectively. Each paste  
139 was poured into the cone immediately after mixing and compacted using a moistened rod. The  
140 cone was lifted vertically, and the diameter of the spread was measured at 30 s.

141 Setting time measurement of pastes was conducted according to the Vicat needle test per  
142 ASTM C191.

143 Reaction heat of pastes were measured at 25 °C using an 8-channel isothermal conduction  
144 calorimeter (TAM Air). Four grams of fresh paste at w/b of 0.5 were loaded.

145 For compressive strength measurement, the pastes were cast into cubic molds with side  
146 length of 20 mm, then sealed, and cured at 25 °C until testing. For each mix proportion, at least  
147 three cubes were measured at each curing age.

148 The hydration of paste samples was stopped at designated ages by immersion of 5 mm-thick  
149 slices in pure isopropanol for at least three days. The samples were vacuum-dried at 40 °C for at  
150 least two days to remove isopropanol, then placed in vacuum desiccator until testing to prevent  
151 carbonation.

152 X-ray diffraction patterns were collected for the samples using a Rigaku Ultima IV  
153 diffractometer operating at 40 kV with 40 mA using a copper target. 15% corundum was blended  
154 into powdered hardened pastes and ground together for quantitative X-ray diffraction (QXRD).  
155 The major phases were quantified by the reference intensity ratio (RIR) method. All scans were  
156 taken from 5° to 75° at a scan rate of 2 °/min.

157 Dried powders were measured using thermogravimetric analysis (TGA) from 30 °C to  
158 1000 °C at a heating rate of 10 °C/min under N<sub>2</sub> protection.

159 Mercury intrusion porosimetry (MIP) was used to probe the pore structure of the pastes at 1  
160 day. The pore size distribution of LC<sup>3</sup> and VC<sup>3</sup> pastes at 1 day was collected from an AutoPore  
161 Iv 9510 porosimeter at a maximum pressure of 414 MPa.

162 Fractured surfaces of hardened pastes after platinum sputtering were imaged using scanning  
163 electron microscopy (NovananoSEM, FEI) at 10 keV under high vacuum. The determination of  
164 C-(A)-S-H composition was obtained by Energy Dispersive X-Ray Spectroscopy (EDS) on  
165 polished samples. The hardened paste was vacuum impregnated in the epoxy resin (EpoKwick,  
166 Buehler) and polished with silicon carbide (SiC) papers (#1200, #2500, and #5000) for 20 min  
167 per level of grit.

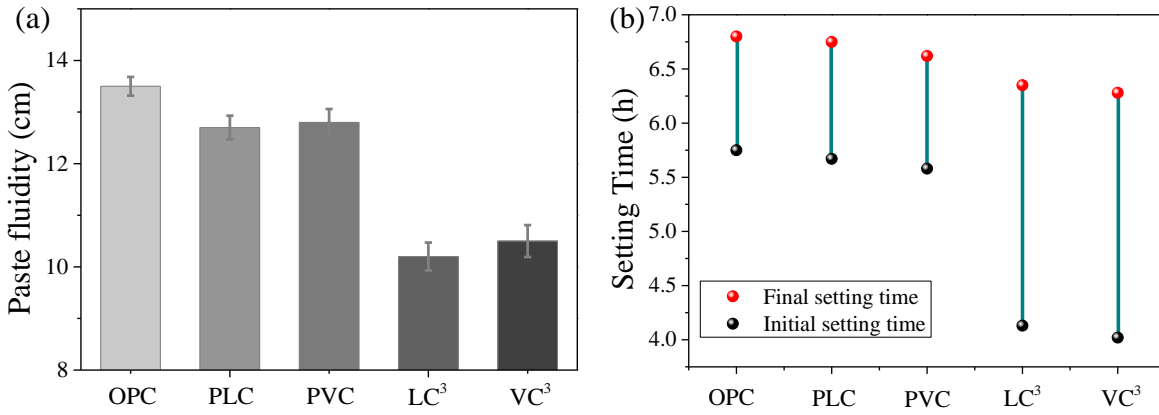
168

### 169 3. Results and analysis

#### 170 3.1 Flowability and setting time

171 With 15% vaterite (D<sub>50</sub> = 5.917 μm) and calcite (D<sub>50</sub> = 5.042 μm) particles, the flowability  
172 of fresh PLC and PVC pastes was ~0.8 cm lower than that of OPC (Fig.3a) due to the finer  
173 particle sizes of CaCO<sub>3</sub> than that of OPC (D<sub>50</sub> = 16.952 μm). Unlike fly ash microspheres,  
174 vaterite microspheres did not promote paste fluidity [25], explained by the high-water demand of  
175 vaterite due to the rough surface texture of vaterite spheres, the porous structure, and  
176 consequently high specific surface area, which was 65.7 m<sup>2</sup>/g for vaterite, compared to 1.3 m<sup>2</sup>/g  
177 for OPC. Compared with PLC, PVC is slightly more flowable due to the presence of vaterite,  
178 benefiting from the spherical particles and a larger D<sub>50</sub> relative to calcite while partially  
179 compromised by the high specific surface area. The flowability of fresh ternary blended cement  
180 pastes, LC<sup>3</sup> and VC<sup>3</sup>, with the presence of 0.2% PCE, was ~2 cm lower than that of OPC. It is  
181 generally agreed that the high-water demand and flocculation induced by the high specific

182 surface area and layered nanostructure of metakaolin results in the poor flowability of LC<sup>3</sup> [15,  
 183 26]. The flowability of VC<sup>3</sup> was ~0.5 cm higher than that of LC<sup>3</sup> due to the presence of vaterite  
 184 microspheres. For the comparison between PLC and PVC, the spherical morphology of vaterite  
 185 helped to improve the fluidity. However, the larger specific surface area of vaterite (65.7 m<sup>2</sup>/g)  
 186 than calcite (2.78 m<sup>2</sup>/g) leads to the negative effect of high-water demand on flowability  
 187 compared with OPC. Under the combined effects, vaterite-blended cements showed higher  
 188 flowability than that of calcite-blended cements. Nevertheless, because the difference in  
 189 flowability of calcite-blended cements and vaterite-blended cements is insignificant, within the  
 190 error range, further research is needed for the rheological properties of vaterite-blended cements.



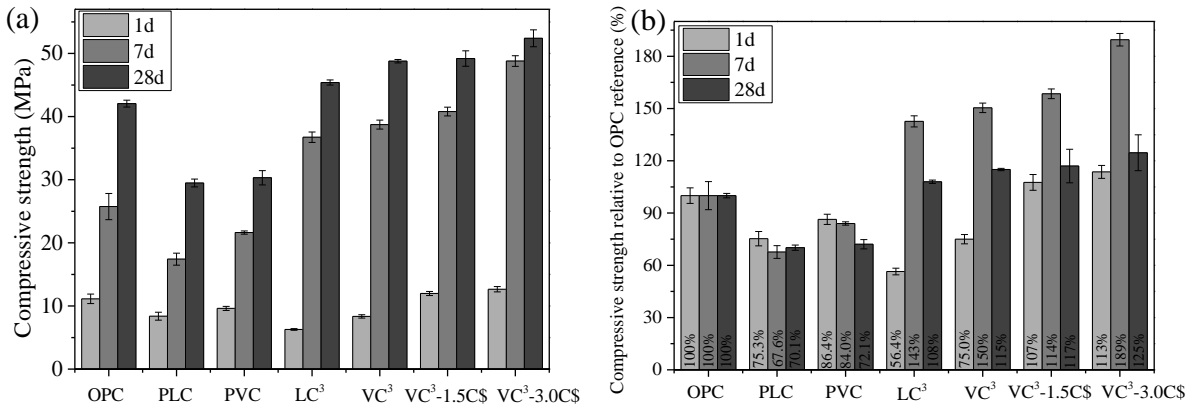
191  
 192 **Fig.3** Workability. (a) Flowability of pastes; (b) Initial and final setting time of pastes.  
 193

194 The initial setting times of PLC and PVC were ~7 min and ~10 min earlier than that of OPC  
 195 (**Fig.3b**), respectively, as explained by the nucleation effect of CaCO<sub>3</sub> [27]. The initial setting  
 196 time of PVC was ~5 min earlier than that of PLC due to the higher degree of hydration  
 197 promotion caused by vaterite than by calcite. The final setting times of PLC and OPC were  
 198 comparable because the dilution effect of calcite is compensated by the reaction between calcite  
 199 and clinker [28-30]. The final setting time of PVC was earlier than that of OPC and PLC due to  
 200 the higher solubility and reactivity of vaterite. The initial and final setting times of LC<sup>3</sup> and VC<sup>3</sup>  
 201 were consistently ~1 h earlier than those of OPC due to accelerated cement hydration by the  
 202 fine metakaolin grains [31]. Compared with LC<sup>3</sup>, the faster initial and final setting of VC<sup>3</sup> may  
 203 additionally be attributed to the higher specific surface area and reactivity of vaterite. More  
 204 details of cement hydration will be explained in later sections.  
 205

### 206 3.2 Compressive strengths

207 **Fig.4** shows that PLC and PVC had lower strength than OPC at the same curing ages due to  
 208 the lower clinker content in the binary cement systems, while PVC showed about 1-4 MPa  
 209 higher strengths than PLC at all ages. The 1-day strengths of LC<sup>3</sup> and VC<sup>3</sup> were 44% and 25%,  
 210 respectively, lower than that of OPC, while the later-age strengths of the ternary cement systems  
 211 were ~8-50% higher than those of OPC. The low 1-day strength of samples without gypsum  
 212 adjustment is consistent with previous findings, in which LC<sup>3</sup> gained ~40-60% 1-day strength of  
 213 OPC depending on the particle size and purity of calcite and metakaolin [10, 14, 32]. Calcite  
 214 shows slightly smaller D50 compared to vaterite but a broader range of particle size distribution.  
 215 In this case, the strength of VC<sup>3</sup> was 7-15% higher than that of LC<sup>3</sup> at all ages, especially at 1  
 216 day. The higher solubility of vaterite (log(K<sub>sp</sub>) = -7.8, 25 °C) relative to calcite (log(K<sub>sp</sub>) = -8.4,  
 217 25 °C) [33] may favor a higher degree of CaCO<sub>3</sub>-clinker reaction in PVC and VC<sup>3</sup> compared to

218 PLC and LC<sup>3</sup>, resulting in significant improvement in 1-day strength by incorporating vaterite  
 219 instead of calcite. Additional replacement of cement by 1.5% and 3% gypsum significantly  
 220 improved the early strength of VC<sup>3</sup>. 1-day strengths of VC<sup>3</sup>-1.5C\$ and VC<sup>3</sup>-3.0C\$ exceeded that  
 221 of OPC by 7% and 13%, respectively, corresponding to 32-38% higher 1-day strengths relative  
 222 to VC<sup>3</sup> without gypsum adjustment. The additional gypsum in VC<sup>3</sup>-3.0C\$ played an important  
 223 role in controlling the rate of aluminates reaction and the formation of more ettringite [34],  
 224 significantly improving the 1-day strengths relative to VC<sup>3</sup>.  
 225

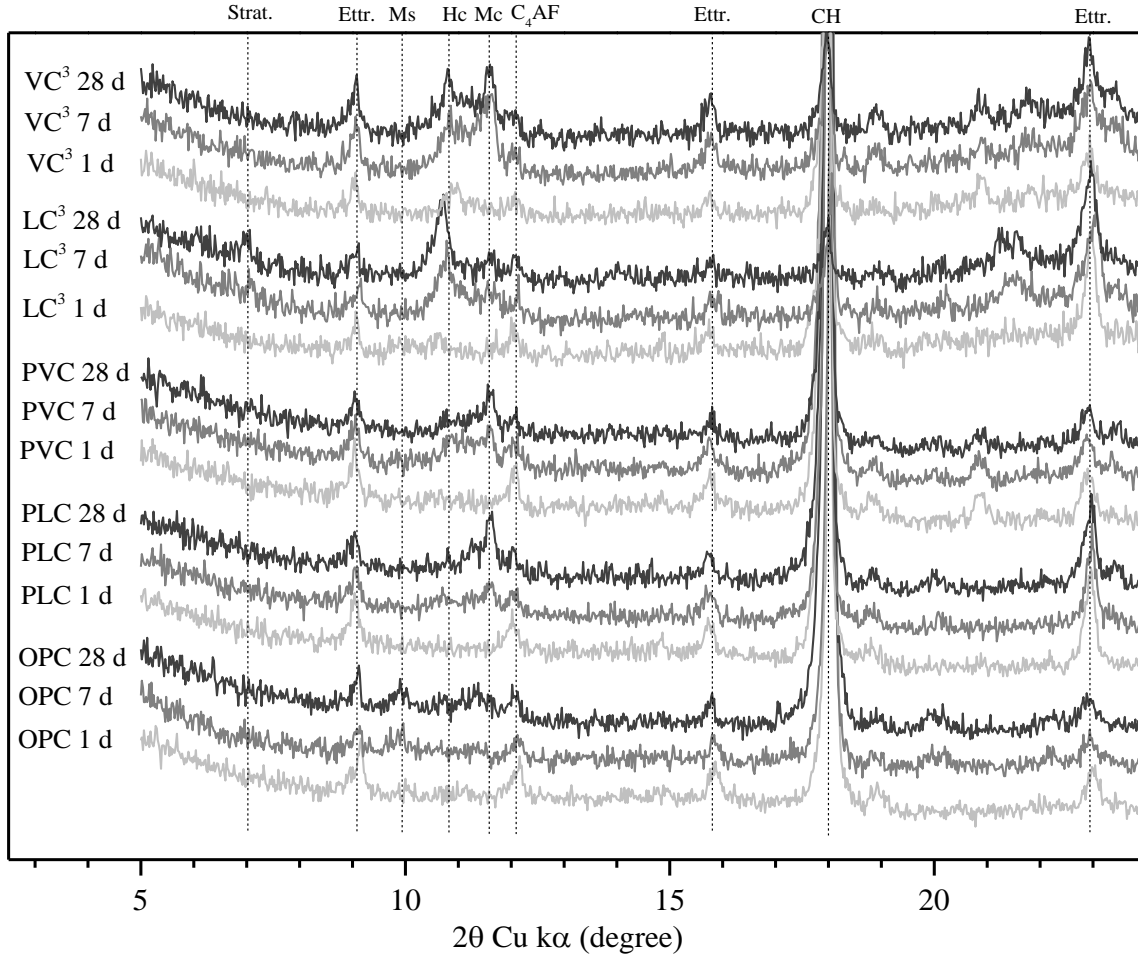


226  
 227 **Fig.4** Compressive strength. (a) Compressive strength of hardened paste; (b) Compressive  
 228 strength of hardened paste normalized to the strength of OPC.  
 229

### 230 3.3 X-ray diffraction

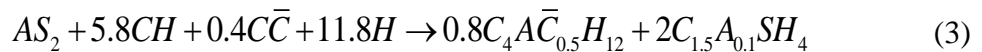
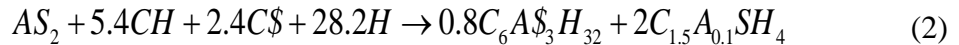
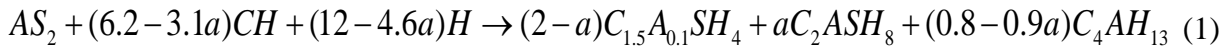
231 The XRD patterns of OPC, PLC, PVC, LC<sup>3</sup>, and VC<sup>3</sup> at 1, 7, and 28 days from 5° to 24° (2θ)  
 232 were shown in Fig.5. The contents of C<sub>3</sub>S, ettringite and carbonate aluminate of samples at 1,7,  
 233 and 28 days were determined by QXRD, shown in **Fig.s1** and **Table s1** (Supplementary  
 234 Information).

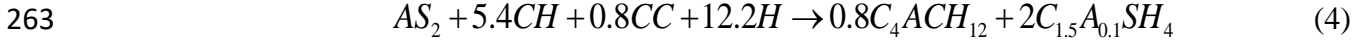
235 **Fig.5** shows that the major crystalline hydration products of OPC were portlandite,  
 236 ettringite, and monosulfoaluminate. For PLC, hemicarboaluminate (Hc) and  
 237 monocarboaluminate (Mc) were observed at 7 days and 28 days, while monosulfoaluminate was  
 238 not observed at any age. More ettringite was stabilized in PLC than OPC. In the presence of  
 239 calcite, the formation of carboaluminate hydrates in PLC occurred after sulfate depletion  
 240 (observed from 7 days) [35], and the predominant formation of Mc due to the low availability of  
 241 Al in PLC. Similarly, Mc was the primary carboaluminate phase in PVC at 7 days and 28 days.  
 242  
 243



**Fig. 5** XRD patterns of OPC, PLC, PVC, LC<sup>3</sup>, and VC<sup>3</sup> at 1, 7, and 28 days. The main crystalline phases include strätlingite (Strät.), ettringite (Ettr.), monosulfoaluminate (Ms), hemicarboaluminate (Hc), monocarboaluminate (Mc), portlandite (CH), vaterite (Va.).

For LC<sup>3</sup>, both Hc and Mc were observed at 7 days and 28 days, along with a decrease in portlandite content. Strätlingite was only observed at 28 days in LC<sup>3</sup>. Hc was the dominant form of carboaluminate in LC<sup>3</sup> despite the presence of a large amount of unreacted calcite [36], consistent with previous studies [10]. During cement hydration, metakaolin reacts with portlandite to form C-A-S-H and strätlingite / calcium aluminate hydrate (C<sub>4</sub>AH<sub>13</sub>) phases (Eq.1) [37, 38]. However, the reaction of metakaolin is greatly influenced by the anions present in the system. With the presence of sulfate, metakaolin reacts with portlandite and sulfate to form ettringite (Eq.2) [39] and further transforms to monosulfoaluminate after sulfate depletion [37]. With the presence of sulfate and calcite, calcite reacts with metakaolin and portlandite to form Hc (Eq.3) after sulfate depletion [40], while ettringite would be stabilized.





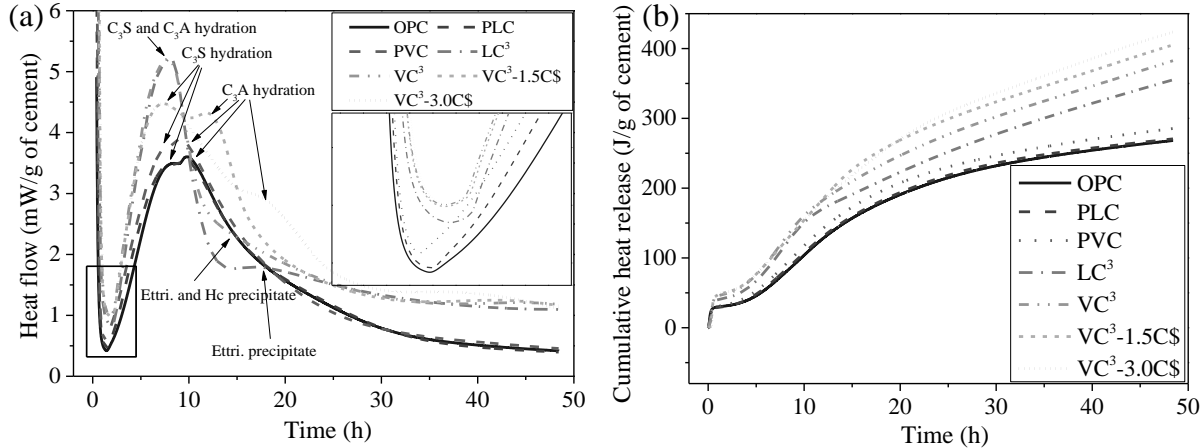
264  
 265 The VC<sup>3</sup> system shows the formation of Hc at 1 day, the formation of Mc at 7 days, and the  
 266 absence of strätlingite at all ages. VC<sup>3</sup> system maintained a higher content of Mc relative to LC<sup>3</sup>  
 267 based on QXRD (**Table s1**, Supplementary Information). Previous studies on LC<sup>3</sup> showed that  
 268 fine calcite particles also resulted in the formation of Hc at 1 day, which remained as the  
 269 primary carboaluminate with secondary Mc at the later ages [41]. Compared with calcite (log  
 270 (K<sub>sp</sub>) = -8.4, 25 °C), the metastable structure and high solubility of vaterite (log (K<sub>sp</sub>) = -7.8,  
 271 25 °C) facilitate the reaction with aluminum phases. Vaterite can react weakly with Al-rich  
 272 phases (e.g., C<sub>3</sub>A and metakaolin) to form a small amount of Hc before sulfate depletion due to  
 273 the higher reactivity of vaterite relative to calcite, supported by the observed Hc in VC<sup>3</sup> and the  
 274 lower ettringite content in VC<sup>3</sup> than LC<sup>3</sup> at 1 day (**Table s1**, Supplementary Information). The  
 275 kinetics of Hc formation is faster than Mc, while Mc is thermodynamically more stable [28, 42].  
 276 Since vaterite is more reactive, its reaction with metakaolin and portlandite seems to favor the  
 277 formation of Mc rather than Hc, supported by the observed weak peak of Hc phase at 1 day and  
 278 strong peak of Mc at 7 days and 28 days in VC<sup>3</sup>. Previous studies demonstrated that strätlingite  
 279 can coexist with calcite in silicate cementitious system [43-45]. For LC<sup>3</sup>, the reaction between  
 280 calcite, MK, and CH is weak due to the low reactivity of calcite (Eq.3). The reaction between  
 281 calcite, MK, and CH reached local equilibrium before 28 days, CH reacted with MK to form  
 282 strätlingite (Eq.1) at 28 days [46]. In contrast, in VC<sup>3</sup>, the highly reactive vaterite participates in  
 283 the reaction with CH and MK (Eq.3 and Eq.4) to form Hc and Mc.

### 284 285 3.4 Heat of hydration

286 **Fig.6a** shows the 48-h isothermal calorimetry results of fresh pastes, normalized to the  
 287 content of Portland cement. Two typical exothermic peaks (C<sub>3</sub>S hydration at ~7.8 h and C<sub>3</sub>A at  
 288 ~9.7 h) were observed in OPC, PLC, and PVC [47]. Only one peak before 10 h was observed in  
 289 LC<sup>3</sup> and VC<sup>3</sup> as the exothermic peak of C<sub>3</sub>A merged into the peak of C<sub>3</sub>S [10], suggesting  
 290 metakaolin-induced accelerated hydration of C<sub>3</sub>A [39]. Both calcite and vaterite increased the  
 291 slope of the acceleration period. Metakaolin further increased the slope of the acceleration period.  
 292 The above evidences suggest that calcite, vaterite, and metakaolin provided extra nucleation sites  
 293 to cement hydration [48]. The induction periods of vaterite-blended cements were shorter than  
 294 those of calcite-blended cements, consistent with the initial setting time results. Existing  
 295 literature has shown elongated induction periods of MK-blended cements than OPC due to the  
 296 addition of PCE [49]. However, in the present study, the initial setting of MK-blended cements  
 297 occurred earlier than that of OPC, supported by the significantly greater slope of its hydration  
 298 acceleration period compared to OPC.

299 In LC<sup>3</sup>, an exothermic peak was detected at 20 h, which was not found in previous results  
 300 [50]. As Hc was not observed in our XRD result of LC<sup>3</sup> at 1 day, and exothermic peak of Hc was  
 301 typically observed during 48-72 h of LC<sup>3</sup> hydration [41], we attribute the exothermic peak at 20  
 302 h to ettringite formation from the reaction between portlandite, sulfate, and highly reactive  
 303 metakaolin (Eq.2). In VC<sup>3</sup>, broad exothermic peaks detected between 12 h and 24 h suggest the  
 304 formation of ettringite and Hc, respectively, supported by XRD results. According to the  
 305 cumulative heat release curve (**Fig.6b**), the order of amount of heat release normalized by  
 306 cement content is OPC<PLC<PVC<LC<sup>3</sup><VC<sup>3</sup>. By comparing PLC versus PVC and LC<sup>3</sup> versus  
 307 VC<sup>3</sup>, vaterite played a critical role in promoting cement hydration in contrast to calcite due to the  
 308 high reactivity and specific surface area of vaterite. Gypsum adjustments (1.5% and 3%)

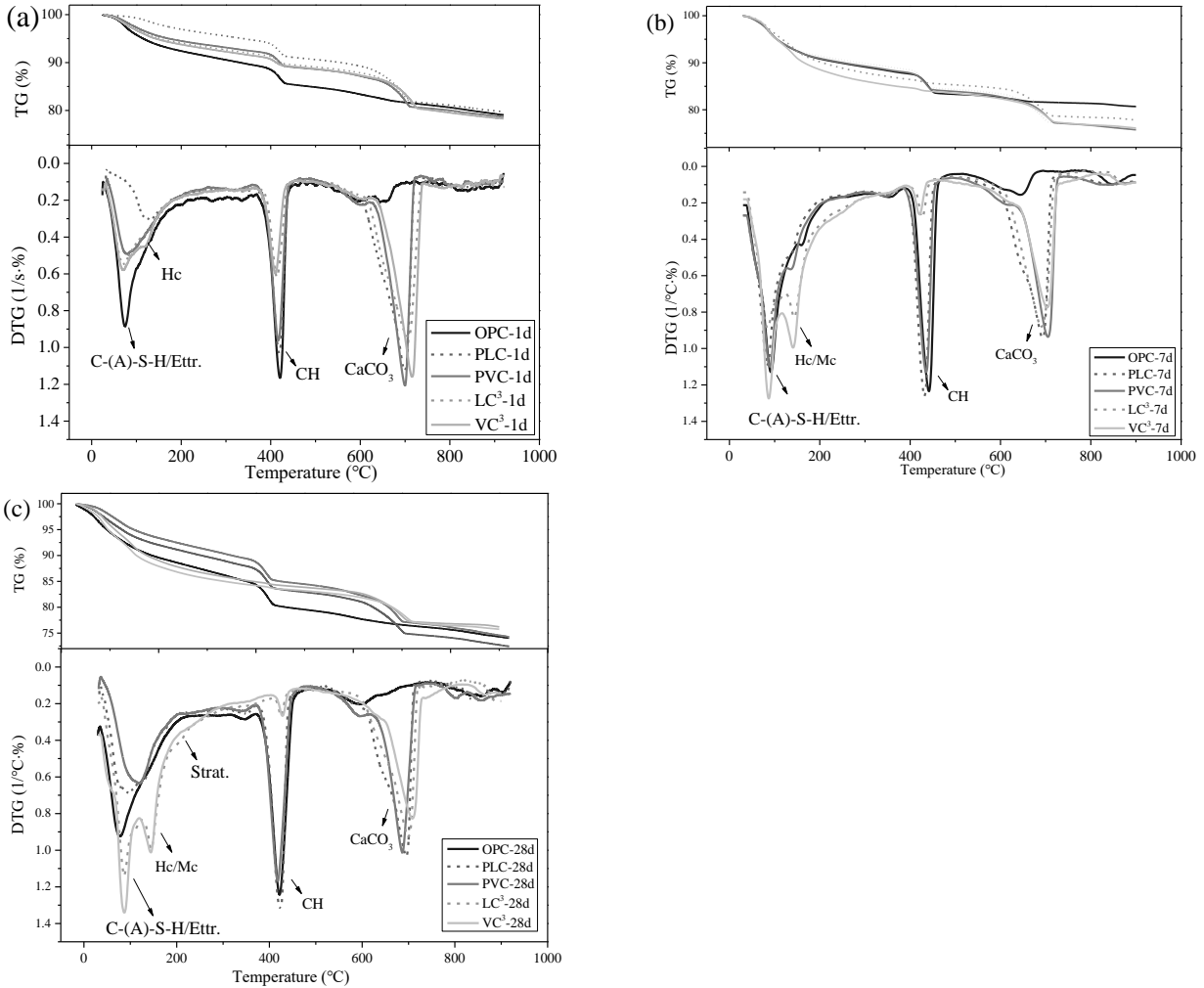
309 decreased the slope of the acceleration period of VC<sup>3</sup>, suggesting retarded C<sub>3</sub>A hydration. The  
 310 retardation effect was more prominent at the higher gypsum content. From the cumulative heat  
 311 release curve, gypsum adjustments reduced the heat release of VC<sup>3</sup> before ~12 h. However, with  
 312 the hydration of aluminates, the heat release of VC<sup>3</sup>-1.5C\$ exceeded that of VC<sup>3</sup> from 12 h, and  
 313 the heat release of VC<sup>3</sup>-3.0C\$ exceeded that of VC<sup>3</sup>-1.5C\$ from 19 h.



314  
 315 **Fig.6** Isothermal calorimetry and cumulative heat release curves of pastes of OPC, PLC,  
 316 PVC, LC<sup>3</sup>, VC<sup>3</sup>, VC<sup>3</sup>-1.5C\$, and VC<sup>3</sup>-3.0C\$. (a) Heat flow; (b) Cumulative heat release.  
 317

### 318 3.5 Thermogravimetric analysis

319 The smaller area of the thermal decomposition peak of portlandite at ~420 °C in **Fig.7a**  
 320 suggests a significant pozzolanic reaction of metakaolin. A thermal decomposition peak at ~123 °C  
 321 was observed in VC<sup>3</sup> at 1 day and assigned to Hc [50], consistent with XRD. This peak was also  
 322 observed in LC<sup>3</sup> and VC<sup>3</sup> at 7 days (**Fig.7b**), assigned to Hc and Mc, respectively, based on the  
 323 XRD results. A thermal decomposition peak of strätlingite at ~ 196 °C [32] was observed in LC<sup>3</sup>  
 324 at 28 days (**Fig.7c**) but not in VC<sup>3</sup> at 28 days, agreeing with our XRD results.



325

326

327

328

329

330

331

332

333

334

335

336

337

338

339

340

341

342

343

344

\*Phase notation: Ettringite (Ettr.), strätlingite (Strät.), hemicarboaluminate (Hc), monocarboaluminate (Mc), portlandite (CH).

**Fig.7** Thermogravimetric analysis of pastes of OPC, PLC, PVC, LC<sup>3</sup>, and VC<sup>3</sup>. (a) at 1 day; (b) at 7 days; (c) at 28 days.

The content of bound water in hydrated pastes was quantified by the mass loss between 40 °C and 450 °C [51]. The tangent method [52] was used to quantify the portlandite content from the dehydration peak between 350 °C and 450 °C as well as CaCO<sub>3</sub> content from the decarbonization peak between 590 °C and 730 °C. The content of bound water and portlandite in each sample was reported in **Table 4**, normalized to anhydrous OPC content, taking into account the clinker content in blended cement systems. Due to the reaction between metakaolin and CaCO<sub>3</sub>, the portlandite content in LC<sup>3</sup> and VC<sup>3</sup> systems was comparable, lower than that in OPC. The bound water content in both LC<sup>3</sup> and VC<sup>3</sup> systems was higher than those in OPC, while VC<sup>3</sup> exhibited a slightly higher bound water content than LC<sup>3</sup>. The differences suggest that calcite, vaterite, and metakaolin promoted cement hydration, and vaterite presented enhanced effectiveness than calcite.

**Table 4** The contents of bound water and portlandite (% of anhydrous OPC weight).

Samples	Bound water	Portlandite
---------	-------------	-------------

	1d	7d	28d	1d	7d	28d
OPC	14.20%	15.90%	24.33%	13.11%	18.28%	18.38%
LC <sup>3</sup>	20.45%	30.19%	33.65%	10.90%	6.17%	1.62%
VC <sup>3</sup>	21.51%	34.44%	35.06%	10.45%	5.83%	1.66%

345

346 The portlandite consumption (CH-Consumption) in LC<sup>3</sup> and VC<sup>3</sup> was calculated by taking  
347 the portlandite content of OPC as the baseline at the same age considering the clinker content,  
348 without considering the accelerated hydration induced metakaolin and CaCO<sub>3</sub>, listed in Table 6.

349 The consumption of metakaolin (MK-Consumption) in LC<sup>3</sup> and VC<sup>3</sup> was calculated based  
350 on the portlandite consumption from TGA using Eq. (2), Eq. (3), and Eq. (4). For calculating  
351 metakaolin content in LC<sup>3</sup> and VC<sup>3</sup> at 1 day, we assumed all portlandite was consumed for the  
352 formation of ettringite (Eq.2) and Hc (Eq.3), respectively. For calculating metakaolin content in  
353 at 7 days and 28 days, we assumed all portlandite in LC<sup>3</sup> was consumed for the formation of Hc  
354 and Mc (Eq.3 and Eq.4), where the mass ratios of Hc to Mc were as determined by QXRD  
355 (Table s1). The calculated reaction degrees of metakaolin were listed in Table 6, which showed  
356 that the reaction degree of metakaolin in VC<sup>3</sup> was higher than that of LC<sup>3</sup> at the same ages. The  
357 reaction degree of MK could be underestimated at early ages, more significantly in VC<sup>3</sup>, because  
358 the calculation in present study did not consider the accelerated hydration induced by metakaolin  
359 and calcite/vaterite.

360 The reaction degree ( $D$ ) of calcite or vaterite in LC<sup>3</sup> and VC<sup>3</sup> can be determined using Eq.5.  
361 As shown in Eq.5, the content of bound water ( $m_{bw}$ ) and unreacted calcite/vaterite ( $m_{CaCO_3}$ ) of  
362 hydrated cement paste was determined using TGA.  $m_s - m_{bw}$  represents the dry mass of the  
363 measured sample (i.e., sample mass  $m_s$  subtracted by  $m_{bw}$ ). Thus, the fraction of unreacted  
364 CaCO<sub>3</sub> over dry mass of the measured sample can be determined. Considering the initial CaCO<sub>3</sub>  
365 content in LC<sup>3</sup> or VC<sup>3</sup> of 15%, the reacted degree of calcite/vaterite can be determined.

$$366 \quad D = 1 - \frac{m_{CaCO_3}}{m_s - m_{bw}} / 15\% \quad (5)$$

367 From the reaction degree of CaCO<sub>3</sub> (Table 5), calcite in LC<sup>3</sup> was barely consumed at 1 day,  
368 by ~11.48% at 7 days, and by ~14.53% at 28 days. Vaterite in VC<sup>3</sup> was consumed by 3.13 %,  
369 21.42%, and 26.44 % at 1 day, 7 days, and 28 days, respectively. The 28-day consumption of  
370 CaCO<sub>3</sub> in LC<sup>3</sup> in this study is higher than the result in [10], due to the finer calcite and higher  
371 w/b used in this study. The consumption of CaCO<sub>3</sub> in VC<sup>3</sup> was higher than that in LC<sup>3</sup> as the  
372 high reactivity of vaterite led to more Mc formation in VC<sup>3</sup>.

373

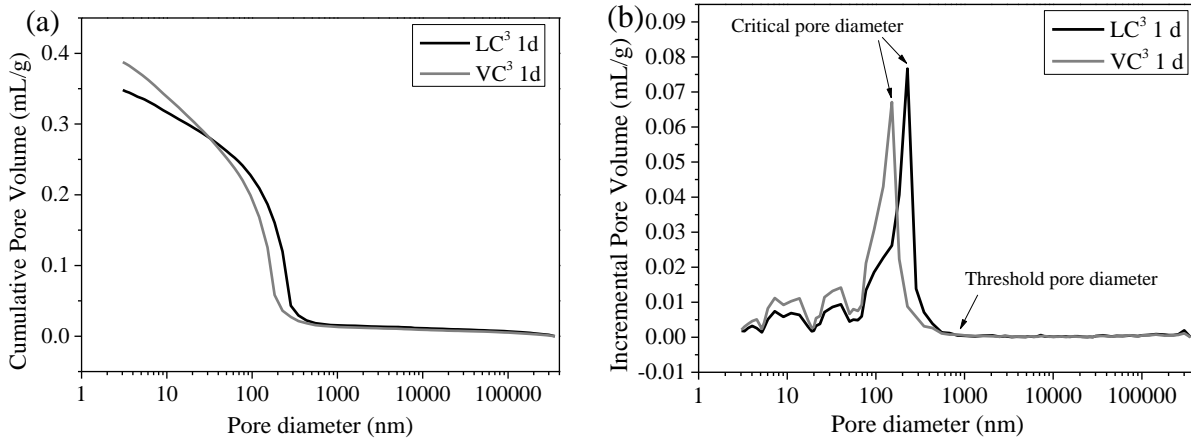
374 **Table 5** The reaction degree of metakaolin (MK-Consumption) and CaCO<sub>3</sub> (CaCO<sub>3</sub>-  
375 Consumption). The consumptions of metakaolin (MK-Consumption) are calculated from Eq.2,  
376 Eq.3 and/or Eq.4, based on the portlandite consumption (CH-Consumption) and the OPC  
377 baseline from TGA. The reaction degree of CaCO<sub>3</sub> (CaCO<sub>3</sub>-Consumption) was calculated based  
378 on TGA.

Sample	CH-Consumption			MK-Consumption			CaCO <sub>3</sub> -Consumption		
	1d	7d	28d	1d	7d	28d	1d	7d	28d
LC <sup>3</sup>	16.8%	66.3%	91.2%	2.24%	11.5%	15.9%	0.31%	11.48%	14.53%

379  
380  
381  
382  
383  
384  
385  
386  
387  
388  
389  
390  
391

### 3.6 Pore structure

The mercury intrusion porosimetry results of LC<sup>3</sup> and VC<sup>3</sup> at 1 day are shown in **Fig. 8**. The total porosities of LC<sup>3</sup> and VC<sup>3</sup> were 43.3% and 48.2%, respectively (**Fig.8a**). The porosity of LC<sup>3</sup> at 1 day is comparable to the result of [41]. The threshold pore diameters of LC<sup>3</sup> and VC<sup>3</sup> were comparable, ~830 nm (**Fig.8b**). The critical pore diameters of LC<sup>3</sup> and VC<sup>3</sup> were 167 nm and 100 nm, respectively. Despite a higher total porosity of VC<sup>3</sup> due to the interior pores of vaterite particles [53], a refined pore microstructure was observed in VC<sup>3</sup>, compared to LC<sup>3</sup>, indicating a higher hydration degree of VC<sup>3</sup> at 1 day, consistent with our calorimeter and thermogravimetry results. Pore size, rather than total porosity, has a more significant influence on the strength of cement-based materials [54]. The refined pore structure of VC<sup>3</sup> at 1 day explains the higher 1-day strength of VC<sup>3</sup> compared with LC<sup>3</sup>.



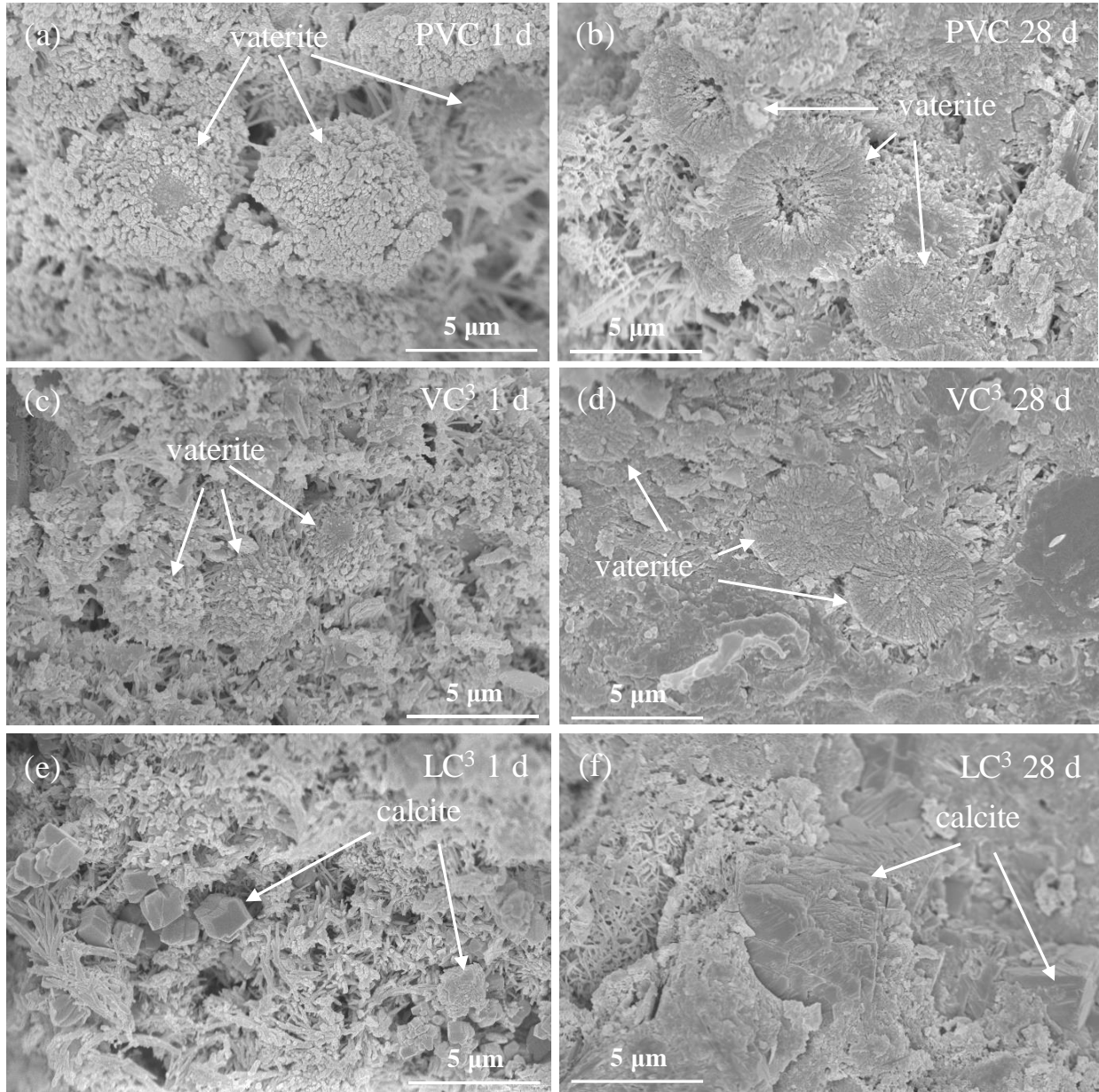
392  
393  
394  
395

**Fig.8** Pore structures of LC<sup>3</sup> and VC<sup>3</sup> at 1 day obtained by mercury intrusion porosimetry. (a) Cumulative pore volume; (b) Incremental pore volume.

### 3.7 Microstructures

Vaterite microspheres were wrapped by hydration products in the hardened paste of PVC and VC<sup>3</sup> at 1 day (**Fig.9a** and **Fig.9c**), while only a small part of calcite surfaces was covered by hydration products in the hardened paste of LC<sup>3</sup> at 1 day (**Fig.9e**). EDS analysis indicates that the surface of vaterite and calcite intermixed with C-(A)-S-H gel at 1 day. At 28 days, vaterite/calcite in PVC, VC<sup>3</sup>, and LC<sup>3</sup> pastes (**Fig.9b**, **Fig.9d**, and **Fig.9f**) were all wrapped by Ca-, Al-, and Si-rich hydration products, i.e., AFm phases (Hc, Mc, and Strätlingite) and C-A-S-H gel, based on the results of EDS, XRD, and TGA. Vaterite microspheres, which were initially hollow before blending, were filled with hydration products, i.e., AFm phases (Hc and Mc) and C-(A)-S-H, at 28 days. This void filling mechanism was not observed in calcite-blended systems due to the solid nature of calcite particles. This difference indicates that pore solution can penetrate porous vaterite microspheres, forming AFm phases (Hc and Mc) and C-(A)-S-H in the interior of vaterite particles, which was more densely filled in VC<sup>3</sup> than in PVC.

408

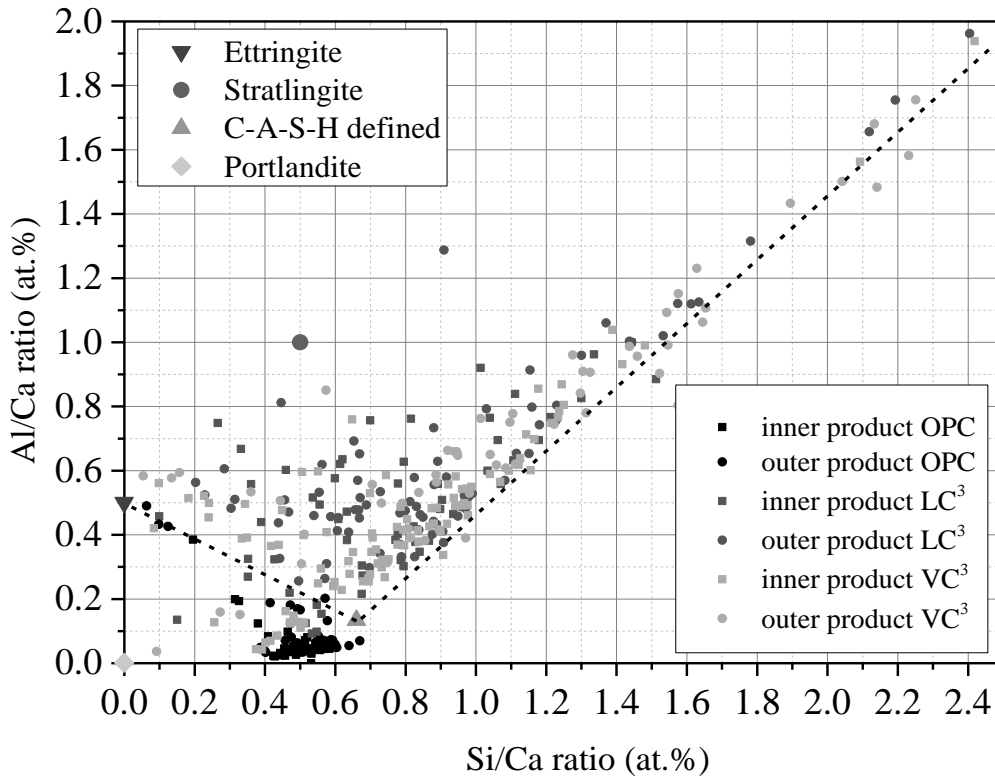


409  
 410 **Fig.9** SEM micrographs showing microstructures of fractured surfaces of PVC, LC<sup>3</sup>, and  
 411 VC<sup>3</sup> at 1 and 28 days. (a) PVC-1 day; (b) PVC-28 days; (c) VC<sup>3</sup>-1 day; (d) VC<sup>3</sup>-28 days; (e)  
 412 LC<sup>3</sup>-1 day; (f) LC<sup>3</sup>-28 days.  
 413

414 When the paste strength was low (e.g., at 1 day), the fracture occurred at the interface  
 415 between vaterite/calcite and hydration products, not through CaCO<sub>3</sub> crystallites. When the paste  
 416 strength was high (e.g., at 28 days), the fracture surface of PVC and VC<sup>3</sup> passed through vaterite  
 417 crystallites. In contrast, the fracture surface of LC<sup>3</sup> at 28 days still appeared at the interface  
 418 between calcite and hydration products. The difference may be explained that the lower density  
 419 of vaterite (~2.54 g/cm<sup>3</sup> compared to ~2.71 g/cm<sup>3</sup> for calcite) and nonuniformity induced by the  
 420 porous hollow structure resulted in the lower strength of vaterite.

421 **Fig.10** shows the Si/Ca molar ratios and Al/Ca molar ratios of C-(A)-S-H of OPC, VC<sup>3</sup>, and  
 422 LC<sup>3</sup>. In **Table 6**, the Si/Ca ratios and Al/Ca ratios of C-(A)-S-H of VC<sup>3</sup> and LC<sup>3</sup> were

423 significantly higher than those of OPC due to the pozzolanic reaction between metakaolin and  
 424 portlandite. In both LC<sup>3</sup> and VC<sup>3</sup>, the outer hydration products exhibited higher Si/Ca ratios and  
 425 Al/Ca ratios than the inner products due to the influence of intermixing with other phases present  
 426 [55]. In LC<sup>3</sup>, the higher reaction degree of metakaolin led to higher Si/Ca ratios and Al/Ca ratios  
 427 of hydration products [42]. Compared with [42, 55], the Si/Ca ratios and Al/Ca ratios of LC<sup>3</sup> in  
 428 this study are slightly higher, likely caused by the higher reaction degree of metakaolin due to  
 429 the high reactivity and purity of metakaolin used in this study. The Si/Ca ratios and Al/Ca ratios  
 430 of the hydration products of LC<sup>3</sup> and VC<sup>3</sup> were comparable, while the average Si/Ca ratios and  
 431 Al/Ca ratios of hydration products of VC<sup>3</sup> were slightly higher than those of LC<sup>3</sup> except for the  
 432 Al/Ca ratios of inner hydration products. This difference indicates that more metakaolin  
 433 participated in the reaction in VC<sup>3</sup>, consistent with our XRD and TGA results.



434 **Fig.10** Processed EDS points analysis obtained on OPC, LC<sup>3</sup>, and VC<sup>3</sup> at 28 days. Al/Ca  
 435 ratio is plotted as a function of Si/Ca ratio (in atomic percentage). C-A-S-H defined represents  
 436  $C_{1.5}A_{0.1}SH_4$  [37].  
 437  
 438

439 **Table 6** Average composition of C-(A)-S-H of OPC, LC<sup>3</sup>, and VC<sup>3</sup> at 28 days.

Molar ratio	OPC		LC <sup>3</sup>		VC <sup>3</sup>	
	Inner product	Outer product	Inner product	Outer product	Inner product	Outer product
Average Si/Ca	0.482	0.505	0.755	0.958	0.791	1.08
Average Al/Ca	0.060	0.107	0.503	0.685	0.482	0.757

440  
 441 4. Discussions

442 Despite excellent mechanical properties and durability [11], LC<sup>3</sup> at ~50% clinker content is  
 443 limited in applications due to low flowability and low 1-day compressive strength [14]. Even

---

444 improved by the sulfate level adjustment, the 1-day strength of LC<sup>3</sup> typically still remains lower  
445 than that of OPC [10, 42, 56]. Alternatively, by using C-S-H seeds to accelerate the early-age  
446 hydration and to improve 1-day strength [18], the workability of LC<sup>3</sup> would be compromised due  
447 to C-S-H seeds-caused fast-setting [57]. Furthermore, C-S-H seeds may lower the late-age  
448 strength of cement-based materials, particularly at low water-to-binder ratios due to self-  
449 desiccation [19]. Moreover, other accelerators also have limited applications in LC<sup>3</sup>: for example,  
450 CaCl<sub>2</sub> would trigger steel rebar corrosion [58]. As now evidenced, the low 1-day strength of LC<sup>3</sup>  
451 could not be easily mitigated without compromising other critical engineering properties. We  
452 emphasize the significance of VC<sup>3</sup> that overcomes this disadvantage of LC<sup>3</sup> – VC<sup>3</sup>, without  
453 compromising late-age strength, has significantly higher 1-day strength than LC<sup>3</sup>, suggesting the  
454 efficacy of VC<sup>3</sup> for practical applications, especially where early-age strength is important. For  
455 the mini slump test, no significant difference in flowability between LC<sup>3</sup> with VC<sup>3</sup> was found.  
456 The altered rheology of VC<sup>3</sup> is worthy of systematic studies. As the microstructure of hardened  
457 paste is refined by vaterite, the potentially improved durability of VC<sup>3</sup> requires validation as well.  
458 As vaterite is more reactive, the influences of varying calcined clay-CaCO<sub>3</sub> ratio deserve equally  
459 high attention.

460 The performance enhancement enabled by using vaterite is mainly attributed to its physical  
461 (high specific surface and nucleation sites) and chemical (high solubility and reactivity)  
462 properties. The physical effect of vaterite is evidenced by the increased hydration rate of clinker  
463 due to the high specific surface area (demonstrated by the heat of hydration measurements). The  
464 chemical effect is manifested by the increased vaterite reaction degree leading to increased C-  
465 (A)-S-H formation (demonstrated with TGA) and by the increased carbonate aluminate  
466 generation (demonstrated with QXRD). In addition, the lower density of vaterite relative to  
467 calcite corresponds to a greater volume of CaCO<sub>3</sub> in VC<sup>3</sup> than LC<sup>3</sup>, resulting in higher degree of  
468 CaCO<sub>3</sub> consumption in VC<sup>3</sup> than in LC<sup>3</sup>. It is worth noting that VC<sup>3</sup> concrete requires slightly  
469 lower binder content by mass than LC<sup>3</sup> concrete due to the lower density of vaterite and higher  
470 strength of VC<sup>3</sup>. As vaterite reacts faster, the VC<sup>3</sup> system may require lower clinker content,  
471 further reducing the embodied carbon footprint. The CO<sub>2</sub> emissions of calcined clay are ~400  
472 kg/ton product [59], while the emissions of vaterite could be nearly neutral or negative  
473 depending on the sources of raw materials and manufacturing technology.

474 Vaterite has been widely used as a filler in chemicals or drug carriers in the biomedical  
475 industry [60, 61] due to its high specific surface areas, high solubility, high dispersion, and low  
476 density [62, 63]. In the construction sector [64], vaterite is used as a key phase in calcium  
477 carbonate cement [65], a promising scalable, low-carbon-footprint binder, due to the polymorph  
478 transition from vaterite to calcite and/or aragonite. However, the use of calcium carbonate  
479 cement, in civil engineering standards, is restricted from wide applications at scale. This fact  
480 jeopardizes the research and development of calcium carbonate cement and the  
481 commercialization of related entities (e.g., novel cement startups) in the field of climate/clean  
482 technology. Compared with LC<sup>3</sup>, the VC<sup>3</sup> system shows higher reactivity and early-age strength.  
483 Thus, VC<sup>3</sup> could potentially become a superior substitute for LC<sup>3</sup> for certain applications. The  
484 enhanced performance of the VC<sup>3</sup> cementitious system paves a way for large-scale utilization of  
485 vaterite and opens a new market for the near-term and long-term operation of the startups. The  
486 strategic utilization of vaterite in VC<sup>3</sup> could help the startups survive in the capital-intensive  
487 construction industry before the approval of calcium carbonate cement for broad applications by  
488 national standards and/or before the wide implementation of carbon credit.

---

489 The phase transformation of vaterite in the environment of hydrated OPC has not been  
490 reported. XRD results suggested that vaterite can stably exist in the OPC, instead of transforming  
491 into calcite or aragonite, likely due to the high alkalinity and high calcium ion content of the  
492 OPC pore solution. We examined the crystalline phase transformation of vaterite by placing it in  
493 a synthetic cement pore solution. The XRD results (Fig.s3, Supplementary Information) confirm  
494 the stable existence of vaterite in cement pore solutions. In addition, as vaterite easily transforms  
495 into calcite in high-humidity environment in the absence of high alkalinity [66], it should be  
496 stored in a sealed condition, similarly as required for cement storage. At present, vaterite can be  
497 prepared at scale by the double decomposition method and carbonization method [67-69]. The  
498 synthesis of high-purity vaterite requires precise control of the pH and reaction time in the  
499 mineralization environment or the addition of polymorph control agents [66, 70], which would  
500 increase production costs. However, the high purity may be unnecessary for usage in  
501 cement/concrete because the impurity carbonates (i.e., calcite, aragonite, and dolomite) also react  
502 with Portland cement and calcined clay [32, 71]. The effects of the vaterite purity on the strength  
503 development and hydration of VC<sup>3</sup> should be explored in the future. Moreover, the low-cost  
504 production of vaterite at the gigaton scale for the construction industry may rely on Ca-rich  
505 byproducts or wastes (e.g., mine tailing and cement kiln dust [21]). The production of vaterite by  
506 mineral carbonization can capture CO<sub>2</sub> directly from the air and/or point source flue gas. For 1  
507 metric ton of CaCO<sub>3</sub> produced, 440 kg of CO<sub>2</sub> could be semi-permanently stored and utilized,  
508 corresponding to up to 100 kg of CO<sub>2</sub> stored in 1 metric ton of VC<sup>3</sup> cement at 1:1 calcined clay-  
509 vaterite ratio and 50% clinker content.

510

## 511 5. Conclusions

512 We developed and demonstrated a new ternary blended cement system, vaterite calcined  
513 clay cement, VC<sup>3</sup>. 45% of ordinary Portland cement was replaced by metakaolin and metastable  
514 CaCO<sub>3</sub> polymorph vaterite at a 2:1 blend. Compared to limestone calcined clay cement, LC<sup>3</sup>,  
515 with a similar particle size distribution, VC<sup>3</sup> exhibited slightly improved flowability and greatly  
516 improved compressive strengths at all ages. With 3% gypsum adjustment, VC<sup>3</sup> presents a 13%  
517 higher strength relative to ordinary Portland cement reference even at 1 day. The outperformance  
518 of VC<sup>3</sup> relative to LC<sup>3</sup> is explained by the metastability and thus higher reactivity of vaterite  
519 relative to calcite. Setting time and heat release measurements demonstrated the faster reaction of  
520 vaterite in VC<sup>3</sup> than limestone (i.e., calcite) in LC<sup>3</sup>. XRD results showed that vaterite reacts with  
521 metakaolin, forming more hemi- and mono-carboaluminate but less strätlingite than in LC<sup>3</sup>. TGA  
522 results suggested that the formation of AFm phases and pozzolanic reaction largely consumed  
523 portlandite. Morphological studies demonstrated that the microstructure of VC<sup>3</sup> was refined in  
524 the presence of vaterite relative to LC<sup>3</sup>, where hollow vaterite resulted in higher bulk porosity of  
525 VC<sup>3</sup> and interior filling with hydration products.

526 Thanks to recent advances in technologies of carbon capture, storage, and utilization (CCUS,  
527 also known as clean/climate technologies), vaterite can be massively produced (potentially 100s  
528 Mt/year) through carbon mineralization with carbon permanently stored at low costs. Besides  
529 vaterite-based cement (e.g., Fortera and Calera), vaterite can be blended to produce VC<sup>3</sup> for  
530 broader applications. The VC<sup>3</sup> system presents a reliable, high-performance complementary  
531 product to LC<sup>3</sup>, particularly when high early-age strengths are required and/or where the LC<sup>3</sup>  
532 productivity is limited by limestone grinding. Therefore, VC<sup>3</sup> shows great promises as an enabler  
533 of CCUS technologies to mitigate climate change at scale.

534

---

535 Acknowledgement

536 This work was performed under the Fundamental Research Funds for the Central  
537 Universities (grant number BLX202006) and the auspices of the U.S. Department of Energy by  
538 Lawrence Livermore National Laboratory (contract No. DEAC52-07NA27344). IM release  
539 number: LLNL-JRNL-849052.

540

541 Contribution statement

542 Yaqiang Li: Methodology, Investigation, Visualization, Writing – original draft, Funding  
543 acquisition.

544 Yue Li: Methodology, Conceptualization, Writing – review and editing.

545 Hongyan Ma: Methodology, Conceptualization, Writing – review and editing.

546 Jiaqi Li: Conceptualization, Methodology, Investigation, Validation, Visualization, Writing –  
547 original draft, Funding acquisition.

548

549 References

550 [1] S.A. Miller, V.M. John, S.A. Pacca, A. Horvath, Carbon dioxide reduction potential in the  
551 global cement industry by 2050, *Cement and Concrete Research* 114 (2018) 115-124.

552 [2] P. Monteiro, S.A. Miller, A. Horvath, Towards sustainable concrete, *Nature Materials* 16(7)  
553 (2017) 698-699.

554 [3] E. Gartner, Industrially interesting approaches to “low-CO<sub>2</sub>” cements, *Cement and Concrete*  
555 *Research* 34(9) (2004) 1489-1498.

556 [4] S.A. Miller, R.J. Myers, Environmental Impacts of Alternative Cement Binders, *Environmental*  
557 *Science & Technology* 54(2) (2020) 677-686.

558 [5] R. Snellings, G. Mertens, J. Elsen, Supplementary Cementitious Materials, *Applied*  
559 *Mineralogy of Cement & Concrete* 74 (2012) 211-278.

560 [6] M.C.G. Juenger, R. Snellings, S.A. Bernal, Supplementary cementitious materials: New  
561 sources, characterization, and performance insights, *Cement and Concrete Research* 122 (2019)  
562 257-273.

563 [7] K. Scrivener, F. Martirena, S. Bishnoi, S. Maity, Calcined clay limestone cements (LC3),  
564 *Cement and Concrete Research* 114 (2018) 49-56.

565 [8] F. Zunino, F. Martirena, K. Scrivener, Limestone Calcined Clay Cements (LC3), *ACI materials*  
566 *journal* 4 (2021) 118.

567 [9] K. Scrivener, F. Avet, H. Maraghechi, F. Zunino, J. Ston, W. Hanpongpun, A. Favier, Impacting  
568 factors and properties of limestone calcined clay cements (LC3), *GREEN MATERIALS* 7(1) (2019)  
569 3-14.

570 [10] M. Antoni, J. Rossen, F. Martirena, K. Scrivener, Cement substitution by a combination of  
571 metakaolin and limestone, *Cement and Concrete Research* 42(12) (2012) 1579-1589.

572 [11] Y. Dhandapani, T. Sakthivel, M. Santhanam, R. Gettu, R.G. Pillai, Mechanical properties and  
573 durability performance of concretes with Limestone Calcined Clay Cement (LC3), *Cement and*  
574 *Concrete Research* 107 (2018) 136-151.

575 [12] M. Sharma, S. Bishnoi, F. Martirena, K. Scrivener, Limestone calcined clay cement and  
576 concrete: A state-of-the-art review, *Cement and Concrete Research* 149 (2021) 106564.

- 
- 577 [13] S. Krishnan, A.C. Emmanuel, V. Shah, A. Parashar, S. Bishnoi, Industrial Production of  
578 Limestone Calcined Clay Cement (LC 3 ) – Experience and Insights, *Green Materials* 7(1) (2018)  
579 15-27.
- 580 [14] R. Hay, L. Li, K. Celik, Shrinkage, hydration, and strength development of limestone calcined  
581 clay cement (LC3) with different sulfation levels, *Cement and Concrete Composites* 127 (2022)  
582 104403.
- 583 [15] O. Canbek, Q. Xu, Y. Mei, N.R. Washburn, K.E. Kurtis, Predicting the rheology of limestone  
584 calcined clay cements (LC3): Linking composition and hydration kinetics to yield stress through  
585 Machine Learning, *Cement and Concrete Research* 160 (2022) 106925.
- 586 [16] USGS, Mineral Commodity Summaries, 2019, :Government Printing Office., 2019.
- 587 [17] P.K. Mehta, P.J. Monteiro, *Concrete Microstructure, Properties and Materials*, New York:  
588 McGraw-Hill., 2017.
- 589 [18] J. Li, W. Zhang, K. Xu, P.J.M. Monteiro, Fibrillar calcium silicate hydrate seeds from  
590 hydrated tricalcium silicate lower cement demand, *Cement and Concrete Research* 137 (2020)  
591 106195.
- 592 [19] M. Wyrzykowski, A. Assmann, C. Hesse, P. Lura, Microstructure development and  
593 autogenous shrinkage of mortars with C-S-H seeding and internal curing, *Cement and Concrete*  
594 *Research* 129 (2020) 105967.
- 595 [20] C.W. Hargis, A. Telesca, P.J.M. Monteiro, Calcium sulfoaluminate (Ye'elimate) hydration in  
596 the presence of gypsum, calcite, and vaterite, *Cement and Concrete Research* 65 (2014) 15-20.
- 597 [21] C.W. Hargis, I.A. Chen, M. Devenney, M.J. Fernandez, R.J. Gilliam, R.P. Thatcher, Calcium  
598 Carbonate Cement: A Carbon Capture, Utilization, and Storage (CCUS) Technique, *Materials*,  
599 2021.
- 600 [22] Y. Mori, T. Enomae, A. Isogai, Preparation of pure vaterite by simple mechanical mixing of  
601 two aqueous salt solutions, *Materials Science and Engineering: C* 29(4) (2009) 1409-1414.
- 602 [23] Q. Shen, H. Wei, Y. Zhou, Y. Huang, H. Yang, D. Wang, D. Xu, Properties of Amorphous  
603 Calcium Carbonate and the Template Action of Vaterite Spheres, *The Journal of Physical*  
604 *Chemistry B* 110(7) (2006) 2994-3000.
- 605 [24] Z. Tan, S.A. Bernal, J.L. Provis, Reproducible mini-slump test procedure for measuring the  
606 yield stress of cementitious pastes, *Materials and Structures* 50(6) (2017) 235.
- 607 [25] B.G. Kutchko, A.G. Kim, Fly ash characterization by SEM–EDS, *Fuel* 85(17) (2006) 2537-2544.
- 608 [26] T.R. Muzenda, P. Hou, S. Kawashima, T. Sui, X. Cheng, The role of limestone and calcined  
609 clay on the rheological properties of LC3, *Cement and Concrete Composites* 107 (2020) 103516.
- 610 [27] E. Berodier, K. Scrivener, Understanding the Filler Effect on the Nucleation and Growth of  
611 C-S-H, *Journal of the American Ceramic Society* 97(12) (2014) 3764-3773.
- 612 [28] T., Matschei, and, B., Lothenbach, and, P. F., Glasser, The role of calcium carbonate in  
613 cement hydration, *Cement and Concrete Research* 37(4) (2007) 551-558.
- 614 [29] Y. Briki, M. Zajac, M.B. Haha, K. Scrivener, Impact of limestone fineness on cement  
615 hydration at early age, *Cement and Concrete Research* 147 (2021) 106515.
- 616 [30] D. Lootens, P. Jousset, L. Martinie, N. Roussel, R.J. Flatt, Yield stress during setting of  
617 cement pastes from penetration tests, *Cement and Concrete Research* 39(5) (2009) 401-408.
- 618 [31] S.E. Schulze, J. Rickert, Suitability of natural calcined clays as supplementary cementitious  
619 material, *Cement and Concrete Composites* 95 (2019) 92-97.

---

620 [32] S. Krishnan, S. Bishnoi, Understanding the hydration of dolomite in cementitious systems  
621 with reactive aluminosilicates such as calcined clay, *Cement and Concrete Research* 108 (2018)  
622 116-128.

623 [33] A.D. Visscher, J. Vanderdeelen, Estimation of the Solubility Constant of Calcite, Aragonite,  
624 and Vaterite at 25°C Based on Primary Data Using the Pitzer Ion Interaction Approach,  
625 *Monatshefte Fur Chemie* 134 (2003) 769–775.

626 [34] H. Huang, X. Li, F. Avet, W. Hanpongpun, K. Scrivener, Strength-promoting mechanism of  
627 alkanolamines on limestone-calcined clay cement and the role of sulfate, *Cement and Concrete*  
628 *Research* 147 (2021) 106527.

629 [35] M. Zajac, A. Rossberg, G. Le Saout, B. Lothenbach, Influence of limestone and anhydrite on  
630 the hydration of Portland cements, *Cement and Concrete Composites* 46 (2014) 99-108.

631 [36] F. Georget, B. Lothenbach, W. Wilson, F. Zunino, K.L. Scrivener, Stability of hemicarbonate  
632 under cement paste-like conditions, *Cement and Concrete Research* 153 (2022) 106692.

633 [37] F. Zunino, Y. Dhandapani, M. Ben Haha, J. Skibsted, S. Joseph, S. Krishnan, A. Parashar,  
634 M.C.G. Juenger, T. Hanein, S.A. Bernal, K.L. Scrivener, F. Avet, Hydration and mixture design of  
635 calcined clay blended cements: review by the RILEM TC 282-CCL, *Materials and Structures* 55(9)  
636 (2022) 234.

637 [38] A. Tironi, M.A. Trezza, A.N. Scian, E.F. Irassar, Thermal analysis to assess pozzolanic activity  
638 of calcined kaolinitic clays, *Journal of Thermal Analysis and Calorimetry* 117(2) (2014) 547-556.

639 [39] M. Maier, S. Scherb, A. Neißer-Deiters, N. Beuntner, K.-C. Thienel, Hydration of cubic  
640 tricalcium aluminate in the presence of calcined clays, *Journal of the American Ceramic Society*  
641 104(7) (2021) 3619-3631.

642 [40] Maciej, Zajac, Anne, Rossberg, Gwenn, Le, Saout, Barbara, Lothenbach, Influence of  
643 limestone and anhydrite on the hydration of Portland cements, *Cement and Concrete*  
644 *Composites*  
645 46 (2014) 99-108.

646 [41] F. Zunino, K. Scrivener, The reaction between metakaolin and limestone and its effect in  
647 porosity refinement and mechanical properties, *Cement and Concrete Research* 140 (2021)  
648 106307.

649 [42] F. Avet, K. Scrivener, Investigation of the calcined kaolinite content on the hydration of  
650 Limestone Calcined Clay Cement (LC3), *Cement and Concrete Research* 107 (2018) 124-135.

651 [43] M.U. Okoronkwo, F.P. Glasser, Stratlingite: compatibility with sulfate and carbonate  
652 cement phases, *MATERIALS AND STRUCTURES* 49(9) (2016) 3569-3577.

653 [44] M.U. Okoronkwo, F.P. Glasser, Stability of stratlingite in the CASH system, *MATERIALS AND*  
654 *STRUCTURES* 49(10) (2016) 4305-4318.

655 [45] M.U. Okoronkwo, F.P. Glasser, Compatibility of hydrogarnet,  $\text{Ca}_3\text{Al}_2(\text{SiO}_4)_x(\text{OH})(4(3-x))$ ,  
656 with sulfate and carbonate-bearing cement phases: 5-85 degrees C, *CEMENT AND CONCRETE*  
657 *RESEARCH* 83 (2016) 86-96.

658 [46] B. Lothenbach, K. Scrivener, R.D. Hooton, Supplementary cementitious materials, *Cement*  
659 *and Concrete Research* 41(12) (2011) 1244-1256.

660 [47] D. Marchon, P. Juilland, E. Gallucci, L. Frunz, R.J. Flatt, Molecular and submolecular scale  
661 effects of comb-copolymers on tri-calcium silicate reactivity: Toward molecular design, *Journal*  
662 *of the American Ceramic Society* 100(3) (2017) 817-841.

---

663 [48] M. Maier, R. Sposito, N. Beuntner, K.-C. Thienel, Particle characteristics of calcined clays  
664 and limestone and their impact on early hydration and sulfate demand of blended cement,  
665 Cement and Concrete Research 154 (2022) 106736.

666 [49] X. Chen, X. Yang, K. Wu, Q. Chen, Z. Yang, L. Xu, H. Li, Understanding the role of C–S–H  
667 seed/PCE nanocomposites, triethanolamine, sodium nitrate and PCE on hydration and  
668 performance at early age, Cement and Concrete Composites 139 (2023) 105002.

669 [50] A. Dixit, H. Du, J. Dang, S.D. Pang, Quaternary blended limestone-calcined clay cement  
670 concrete incorporating fly ash, Cement and Concrete Composites 123 (2021) 104174.

671 [51] K. De Weerd, M.B. Haha, G. Le Saout, K.O. Kjellsen, H. Justnes, B. Lothenbach, Hydration  
672 mechanisms of ternary Portland cements containing limestone powder and fly ash, Cement and  
673 Concrete Research 41(3) (2011) 279-291.

674 [52] B.K. Marsh, R.L. Day, Pozzolanic and cementitious reactions of fly ash in blended cement  
675 pastes, Cement and Concrete Research 18(2) (1988) 301-310.

676 [53] T. Beuvier, B. Calvignac, G.J.-R. Delcroix, M.K. Tran, S. Kodjikian, N. Delorme, J.-F. Bardeau,  
677 A. Gibaud, F. Boury, Synthesis of hollow vaterite CaCO<sub>3</sub> microspheres in supercritical carbon  
678 dioxide medium, Journal of Materials Chemistry 21 (2011) 9757–9761.

679 [54] Y. Dhandapani, M. Santhanam, Assessment of pore structure evolution in the limestone  
680 calcined clay cementitious system and its implications for performance, Cement and Concrete  
681 Composites 84 (2017) 36-47.

682 [55] F. Avet, X. Li, K. Scrivener, Determination of the amount of reacted metakaolin in calcined  
683 clay blends, Cement and Concrete Research 106 (2018) 40-48.

684 [56] O. Akhlaghi, T. Aytas, B. Tatli, D. Sezer, A. Hodaei, A. Favier, K. Scrivener, Y.Z. Menciloglu, O.  
685 Akbulut, Modified poly(carboxylate ether)-based superplasticizer for enhanced flowability of  
686 calcined clay-limestone-gypsum blended Portland cement, Cement and Concrete Research 101  
687 (2017) 114-122.

688 [57] C. Bhojaraju, M. Charrier, C.M. Ouellet-Plamondon, How Admixtures Affect Yield Stresses  
689 of Cement, ACI materials journal (6) (2021) 118.

690 [58] A. Poursaee, A. Laurent, C.M. Hansson, Corrosion of steel bars in OPC mortar exposed to  
691 NaCl, MgCl<sub>2</sub> and CaCl<sub>2</sub>: Macro- and micro-cell corrosion perspective, Cement and Concrete  
692 Research 40(3) (2010) 426-430.

693 [59] Y. Cancio Díaz, S. Sánchez Berriel, U. Heierli, A.R. Favier, I.R. Sánchez Machado, K.L.  
694 Scrivener, J.F. Martirena Hernández, G. Habert, Limestone calcined clay cement as a low-carbon  
695 solution to meet expanding cement demand in emerging economies, Development Engineering  
696 2 (2017) 82-91.

697 [60] D.B. Trushina, T.V. Bukreeva, M.V. Kovalchuk, M.N. Antipina, CaCO<sub>3</sub> vaterite microparticles  
698 for biomedical and personal care applications, Materials Science and Engineering: C 45 (2014)  
699 644-658.

700 [61] L.-H. Fu, C. Qi, Y.-R. Hu, C.-G. Mei, M.-G. Ma, Cellulose/vaterite nanocomposites:  
701 Sonochemical synthesis, characterization, and their application in protein adsorption, Materials  
702 Science and Engineering: C 96 (2019) 426-435.

703 [62] W. Li, C. Gao, Efficiently Stabilized Spherical Vaterite CaCO<sub>3</sub> Crystals by Carbon Nanotubes  
704 in Biomimetic Mineralization, Langmuir 23(8) (2007) 4575-4582.

---

705 [63] J. Feng, G. Wu, C. Qing, Biomimetic synthesis of hollow calcium carbonate with the  
706 existence of the agar matrix and bovine serum albumin, *Materials Science Engineering C* 58  
707 (2016) 409-411.

708 [64] O. Cherkas, T. Beuvier, F. Zontone, Y. Chushkin, L. Demoulin, A. Rousseau, A. Gibaud, On  
709 the kinetics of phase transformations of dried porous vaterite particles immersed in deionized  
710 and tap water, *Advanced Powder Technology* 29(11) (2018) 2872-2880.

711 [65] P.J.M. Monteiro, L. Clodic, F. Battocchio, W. Kanitpanyacharoen, S.R. Chae, J. Ha, H.-R.  
712 Wenk, Incorporating carbon sequestration materials in civil infrastructure: A micro and nano-  
713 structural analysis, *Cement and Concrete Composites* 40 (2013) 14-20.

714 [66] R. Ševčík, M. Pérez-Estébanez, A. Viani, P. Šašek, P. Mácová, Characterization of vaterite  
715 synthesized at various temperatures and stirring velocities without use of additives, *Powder*  
716 *Technology* 284 (2015) 265-271.

717 [67] D. Konopacka-Łyskawa, *Synthesis Methods and Favorable Conditions for Spherical Vaterite*  
718 *Precipitation: A Review*, *Crystals*, 2019.

719 [68] S. Kim, J. Jeon, M.-J. Kim, Vaterite production and particle size and shape control using  
720 seawater as an indirect carbonation solvent, *Journal of Environmental Chemical Engineering*  
721 10(2) (2022) 107296.

722 [69] X. Liu, B. Wang, Z. Zhang, Z. Pan, H. Cheng, F. Cheng, Glycine-induced synthesis of vaterite  
723 by direct aqueous mineral carbonation of desulfurization gypsum, *Environmental Chemistry*  
724 *Letters* 20(4) (2022) 2261-2269.

725 [70] Y. Sheng Han, G. Hadiko, M. Fuji, M. Takahashi, Crystallization and transformation of  
726 vaterite at controlled pH, *Journal of Crystal Growth* 289(1) (2006) 269-274.

727 [71] Y. Dhandapani, M. Santhanam, G. Kaladharan, S. Ramanathan, Towards ternary binders  
728 involving limestone additions — A review, *Cement and Concrete Research* 143 (2021) 106396.  
729